EFFECTS OF MILLING TEMPERATURE AND TIME ON PHASE EVOLUTION OF Ti-BASED ALLOY

F. Kristaly [a], M. Sveda [b], A. Sycheva [b], T. Miko [c], A. Racz [d], G. Karacs [b], D. Janovszky [b,*]

[a] Institute of Mineralogy and Geology, University of Miskolc, Hungary
[b] MTA-ME Materials Science Research Group ELKH, Miskolc, Hungary
[c] Institute of Physical Metallurgy, Metalforming and Nanotechnology, University of Miskolc, Hungary
[d] Institute of Raw Material Preparation and Environmental Processing, University of Miskolc, Hungary

Abstract

$Ti_{50}Cu_{25}Ni_{20}Sn_5$ (at.%) powder was subjected to high-energy ball milling at room temperature and -78 °C. As a function of the milling time, evaluation of phases, morphology, and the refinement of grain size were investigated by scanning electron microscopy (SEM) and X-ray diffraction analysis (XRD), differential scanning calorimetry (DSC), transmission electron microscopy (TEM), and laser-diffraction particle size analysis (PSA). The transformation of the crystalline structure into an amorphous structure and then the transformation into a nanocrystalline structure during further milling was detected. The stress-induced martensitic transformation occurred after 30 min milling time at both temperatures, the cubic $Cu(Ni,Cu)Ti_2$ phase transformed into the orthogonal structure. The hardness value of powders after 150 min milling time increased from 506 to 780 $HV_{0.01}$. The milling temperature did not significantly influence the amount of amorphous fraction (33-36 wt.%), however, the composition of amorphous content was more influenced by temperature. The interval of crystallite size was between 1.2 and 11.7 nm after 180 min of milling. The amount and the cell parameters of the Sn-containing phases were different for the two milling experiments because the diffusion coefficients of the Sn atom differed to a large extent.

Keywords: Amorphous-nanocrystalline composites; Ti-based bulk metallic glasses; Ball milling; Powder metallurgy; Microstructure

1. Introduction

Lightweight Ti has excellent high-corrosion resistance and biocompatibility. Owing to increasingly demanding lightweight applications, the tensile strengths of Ti alloys should be further improved. Ti-based amorphous alloys have ultrahigh strength and hardness [1-5]. In the field of industrial use, one expects a material with high tensile strength and high tensile ductility. Unfortunately, the multiplication of strength and ductility is constant. The composites prove the solution-nanosized particles dispersed in an amorphous-nanocrystalline matrix [6-9].

Amorphous metals with nanostructured particles can be produced by different techniques. High energy ball-milling, one of the non-equilibrium processing techniques, has been often used for preparing a wide range of metastable materials such as amorphous and nanocrystalline materials [10-11]. The most important event is a ball-powder collision, which ensures repeated severe plastic deformations [12] and fracture processes leading to the increase of lattice defects, crystallite refinement, and reaching nanosized or amorphous structures and phase transformations [13-15]. Due to repeated fracturing, cold welding, and re-fracturing of particles, new chemically active surfaces are developed and solid-state interdiffusion, supersaturation beyond the equilibrium limit can take place [16, 17]. Mechanical activation of the grain surfaces is also playing an important role in chemical processes.

The milling temperature has a significant effect on the mechanical milling process of an alloy system. At extremely low temperatures, the plastic deformation is limited and we expect a finer grain size. There have been only a few investigations reported where the grinding bowl or material is cooled with dry ice [18]. The decreased diffusivity and accelerate fracturing effects at lower temperatures of milling may be favorable to our aim of producing an amorphous metal with nanostructured particles. Two consecutive designs of experiments were carried out. In the first experiment, the high-energy milling was realized at room temperature. In the current experiment around the grinding bowl applied dry ice cooling in order to

investigate the effect of temperature on the study of the process of phase transformations during high energy milling.

The transformation of crystalline phases in similar research was not investigated in detail, only at the level of amorphous phase generation and the disappearance of crystalline components [20, 21, 22, 23]. Although the development of new crystalline phases by mechanical alloying (MA) is frequently examined (by XRD or TEM), the transformations caused by mechanical milling (MM) are mostly disregarded. Powder XRD is a suitable method to analyze larger volumes of MM samples, giving an average result for all particle (crystallite) characteristics. With this method, applying Rietveld refinement, it is possible to quantify the developed amorphous content, as well as the type and amount of amorphized crystalline phases, while we get direct information on crystallite size, lattice distortions (strain), and lattice changes due to chemical substitutions. Since the XRD peaks of major phases are located in a narrow 2θ angular range, peak broadening leads to severe overlapping. Without the use of Rietveld refinement and direct deconvolution, phase analysis of such materials is not possible.

This work is focused on the synthesis of Ti-based amorphous and nanocrystalline composites. Ti-based bulk amorphous alloy with $Ti_{50}Cu_{25}Ni_{20}Sn_5$ composition was chosen, the first time produced with casting [19]. Our aim was to obtain a similar amorphous alloy by high-energy ball milling.

2. Experimental conditions

Master alloy ingot with a composition $Ti_{50}Cu_{25}Ni_{20}Sn_5$ (at. %) was prepared by arc melting of pure metal mixtures (min. 99.9 wt.%) with a Ti-getter under a purified argon atmosphere. The ingots were machined by a turning mill into chips. A tungsten carbide tool without any lubricant was used. Based on the XRD patterns and SEM analysis, five phases were identified in the master alloy [24]: Cu(Ni, Cu)Ti$_2$ phase with cubic and orthorhombic structure, hexagonal a-Ti phase, hexagonal (Sn, Cu, Ni)Ti$_3$ phase, and tetragonal (Cu, Sn)Ti$_3$ (Table 1). The machined chips were fractionated to a particle size below 320 μm for planetary ball milling. Amorphous/nanostructured powders were obtained in a Pulverisette 5 high-energy planetary ball mill under a protective argon atmosphere using a 250 ml stainless steel vial and balls. The weight ratio of the ball to the powder (BPR) and rotational speed were set to 80:1 and 200 rpm, respectively. The initial weight of the milling material was 6.40 g. The diameters of the hardened steel balls were 20 mm, 15 mm, 10 mm, 5 mm, and 2.5 mm. A sample of 0.5 g was taken every 30 minutes to check the effect of the milling time on the particle size and shape, and the amorphous content.

The microstructure of powders was examined by a Hitachi S-4800 Scanning Electron Microscope (SEM) equipped with a BRUKER AXS type energy-dispersive X-ray spectrometer (EDS). The particle size distribution of the ground material was determined by a Horiba LA-950 V2 type laser-diffraction particle size analyzer (LPSA) in distilled water. Thermal analysis was performed in a Netzsch 204 DSC at a heating rate of 0.66 K/s under a flow of purified argon.

The composition of samples was examined with a Bruker D8 Advance diffractometer (XRD) using Cu Kα radiation (40 kV, 40 mA), in parallel beam geometry obtained with a Göbel mirror equipped with a Vantec-1 position sensitive detector (1° window opening), measured in the 2-100 °(2θ) angular range, at a 0.007° (2θ)/29-sec speed. The specimen was rotated in the sample plane during the measurement to obtain data from the whole surface and to reduce in-plane preferred orientation effects. The quantitative results were obtained by the combined use of Rietveld refinement and peak area calculation (Pawley fit). The amorphous fraction was determined using peak area determination from the Pawley fit in TOPAS4 (amorphous hump method). Crystallite sizes were calculated from peak broadening by Scherrer equation after correction for instrumental contribution, during the Rietveld refinement. The instrumental profile was calculated by the empirical parametrisation method using NIST 640d Si powder as standard. The background was fitted by the use of Chebyshev polynomial 4th degree and hyperbola (1/x) function for air scattering at low angles. For each phase, a fitting pattern was calculated from initial unit cell values and atomic coordinates from ICSD database or relevant literature. During the refinement unit cell parameters and crystallite sizes were fitted to estimate the actual values. Due to the parallel beam geometry, sample displacement, surface roughness and other errors were eliminated and needed no correction, also making calculation errors minimal. The peak broadening was resolved by simultaneous size and strain calculation (size (nm) = FWHM(2θ)*cos(θ)/λ and $\varepsilon 0$ = FWHM(2θ)/(4tanθ), a dimensionless parameter which could be related to distortion of lattice parameters in percent.)

For nanoscale insight, transmission electron microscopy (FEI Tecnai G2 TEM, LaB$_6$ field emission gun, 200 kV accelerating voltage) on powder specimens prepared by the suspension droplet method on Lacey carbon-coated Cu-grids was used. Bright-field images and diffraction were recorded on an Eagle 2k CCD camera, the camera length of the electron diffraction was 550 mm.

The microhardness measurements were performed by Instron Tukon 2100B equipment, applying a load of 10 g for 15 s for milled powders. The powder

samples were embedded in acrylic resin and polished to produce a surface suitable for micro indenting. Only symmetric indenting marks were used to calculate HV0.01 values to avoid misleading results from the indenting of aggregates.

3. Results and discussion
3.1. Microstructural observations

A very strong size-shaped anisotropy was observed in the as-received machined chips (Fig. 1). The thin lamellas of chips with a "sawtooth" like shape are stuck to each other. The average thickness and length of the chips were ~30 µm and ~500 µm, respectively. The hardness of the chips was $HV_{0.01}$ 506. After 30 min of ball milling, the sub-particles became separated into flattened, thin disk-shaped particles due to the shearing effect of the balls (Fig.1). The "sawtooth" shape observed on the primary chip particles disappeared, indicating that only a detachment of thin lamellar sub-particles occurred without further shearing or deformation. The shape of the particles was still angular, with minimal rounding of the corners and edges.

The effect of temperature on the variation of powder morphology as a function of the milling time (Fig.1) was conspicuous. From 60 min up to 120 min of ball milling at room temperature the shape of particles changed to a spherical one, with significant rounding and deformation of lamellar particles. After 150 min of ball milling the shape of particles changed again to the flattened thin disk-shaped ones due to the shearing effect of balls which destroyed the aggregates (Fig. 1).

The small thin lamellar particles were liberated from the spherical aggregates. In contrast, the aggregation of particles was first observed at 120 min of milling at – 78 °C (Fig.1). The characteristic morphology was lamellar shape up to 180 minutes of milling at this temperature. It seems that the efficiency of cold-welding was diminished by reducing the milling temperature and the particle size dropped faster than during the room temperature milling.

The particle size distribution of milled powder at two temperatures confirmed this observation. The distributions of room temperature milled material were symmetric, except for raw material and the 30 min sample (Fig.2a). In these two cases, the particle distribution was bi-modal; the particle size ratio smaller than the mode was significant. It is worth noting, that the mode increased after 150 min, the cold-welding was the determining factor causing the increase in particle size in this period. Slightly bi-modal distribution could also be seen at -78 °C milling (Fig.2b). Up to 30 min of milling time, the range of particles smaller than the mode size existed in the case of both milling processes, as it was mentioned earlier.

The situation reversed after 60 min milling with dry ice. The range of particles greater than the mode size was well-observed and it persisted. Observing the mode of particle size, it can be established, that the fragmentation took place faster in the case of milling with dry ice cooling (Fig.2c) and the mode was near-constant after 120 min, 45 µm, and 25 µm milling at room temperature and -78 °C, respectively.

3.2. Phase evaluation and hardness during the milling process

The phase evolution of powders occurring by ball milling was screened by Rietveld refinement. The phase determinations for $Ti_{50}Cu_{25}Ni_{20}Sn_5$ after 30 min of milling are shown in Fig. 3, by plotting the calculated signal patterns of phases and the difference pattern which showed the quality of fitting. In the amorphous and crystalline phases, the deformation occurred differently. The amorphous phase had high strength, however, the ductility was generally low. In an amorphous-crystalline composite, the crystalline phases ensured ductility. Therefore, it was very important to know the fraction of the crystalline phase. On the starting powders, crystalline phases were identified from the ICDD PDF2 database, as $SnTi_3$ (PDF 65-3527), Ti (hexagonal, 44-1294), and $CuNiTi_2$ (cubic, 52-0860). During the Rietveld refinement, the unit cell parameter values were used to infer alloying element content, based on the cited literature [25-32], as listed in Table 1. The phases with multiple alloying elements were not found in the ICDD database, they were inferred by Rietveld refinement from the starting crystal structures, based on literature data. The most important process was the evolution of the ultrafine-grained and amorphous phase(s), based upon which some stages of reactions should be delimited (Table 1):

Period I: from 0 to 30 min as activation period, particle and crystallite (grain) size decrease dominated. The cubic $Cu(Ni,Cu)Ti_2$ phase transformation to an orthorhombic structure was significant, with minor amorphization in both milling processes (Table 1);

Period II: from the 30 to 120 min period, the crystallite size decreased under 100 nm; the crystal defects increased due to the high energy storage, the amorphization reached the maximum content of 36 wt.% and 33 wt.% at room temperature and -78 °C milling, respectively (Table 1).

Period III: over 120 min as a mechanical crystallization period, the amorphous and nanocrystalline phases transformed into each other at -78 °C milling (Table 1). However, the process was only one-way at room temperature milling, the amorphous phase became a nanocrystalline structure.

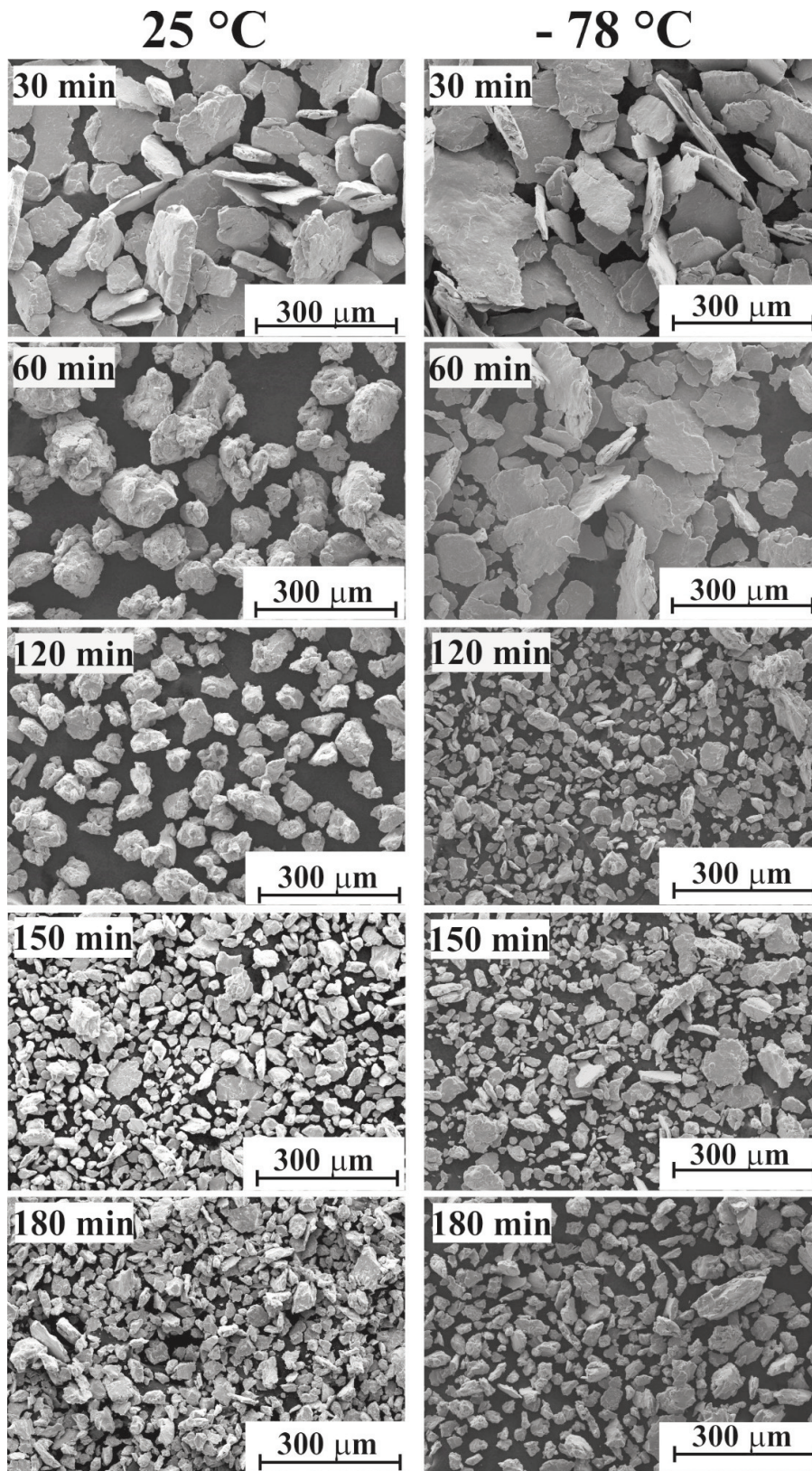The amount of some crystalline phases was changing in a fluctuant manner (Table 1), which was

25 °C   **- 78 °C**

Figure 1. The morphological variation on scanning electron microscopic (SEM) images for $Ti_{50}Cu_{25}Ni_{20}Sn_{5}$ particles milled for different time and temperature
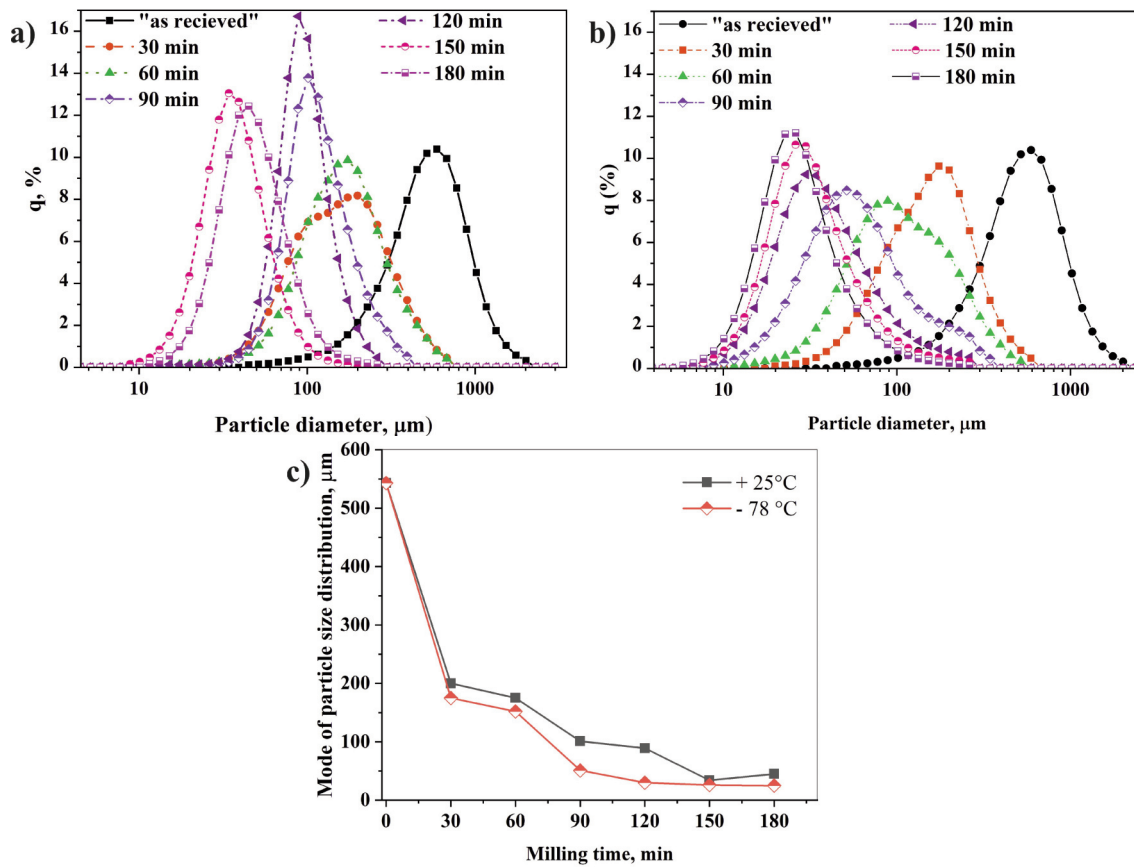
Figure 2. *Particle size distribution (a)+25 °C, (b)-78 °C and mode of $Ti_{50}Cu_{25}Ni_{20}Sn_5$ powders after different milling times*
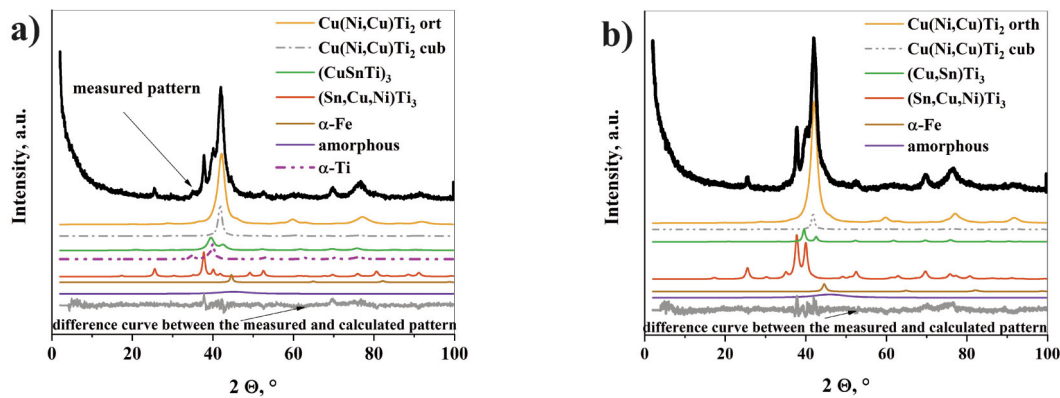

Figure 3. *X-ray diffraction pattern of milled powder with 30 min at (a) 25°C, (b) -78°C*

strongly related to the element exchange between the ultrafine phases and the resulting small chemical variations in the composition of each phase. As indicated by unit cell parameters (Table 1), the chemical compositions constantly changed, which would require the definition of a new phase in each milling step. However, the crystal structure was not affected strongly enough to define a new phase, peak positions were shifted with minimal values, like in

alloy structures. Thus, the fluctuant quantity variation was connected to the interchange of elements by diffusion between crystalline phases and the development of multiple nanocrystalline sub-phases (different in chemistry only, not in the crystal structure). The sub-phases were consumed by amorphization, but in the next stage, new sub-phases could develop, with a different chemical composition in a similar crystal structure. These ultrafine

Table 1. *Features of crystallites based on the XRD of the milled powder structure in the case of Ti$_{50}$Cu$_{25}$Ni$_{20}$Sn$_5$ alloy (errors for lattice parameters are < 0.0001 thus not reported here)*

Phase		milling time, min	0	30	60	90	120	150	180
cubic Cu(Ni, Cu)Ti$_2$ space group Pm-3m	-78 °C	a, nm	0.3050	0.3054	0.3054	0.3082	0.3100	0.3074	0.3069
		crystallite size, nm	21±2	10 ±2	4 ±1	3 ±1	2 ±1	2 ±1	2 ±1
		wt% Rietveld	53.0	9.7	3.6	4.1	3.0	1.8	4.0
	+25°C	a, nm	0.3050	0.3054	0.3089	0.3082	0.3100	0.3074	0.3069
		crystallite size, nm	21±2	8 ±2	4 ±1	2 ±1	2 ±1	3 ±1	3 ±1
		wt% Rietveld	53.0	13.0	6.6	4.1	1.6	1.0	0.8
orthorhombic Cu(Ni, Cu)Ti$_2$ space group Pmmb	-78°C	a, nm	0.2990	0.2950	0.2950	0.2950	0.2850	0.2850	0.2850
		b, nm	0.4330	0.4300	0.4300	0.4300	0.4300	0.4300	0.4300
		c, nm	0.4460	0.4450	0.4450	0.4450	0.4450	0.4450	0.4450
		crystallite size, nm	13 ±3	5 ±1	3 ±1	2 ±1	2 ±1	2 ±1	2 ±1
		wt% Rietveld	13.3	54.7	31.4	37.6	34.4	28.6	29.1
	+25°C	a, nm	0.2990	0.2950	0.2950	0.2950	0.2907	0.2850	0.2850
		b, nm	0.4330	0.4300	0.4300	0.4300	0.4300	0.4300	0.4300
		c, nm	0.4460	0.4450	0.4450	0.4450	0.4450	0.4450	0.4450
		crystallite size, nm	13 ±3	5 ±1	2 ±1	2 ±1	2 ±1	~1.0	~1.0
		wt% Rietveld	13.3	33.4	24.8	31.3	34.5	35.0	25.7
hexagonal α-Ti(Cu) s pace group P63/mmc	-78°C	a, nm	0.2970	-	-	-	-	-	-
		c, nm	0.4700	-	-	-	-	-	-
		crystallite size, nm	8 ±2	-	-	-	-	-	-
		wt% Rietveld	13.7	-	-	-	-	-	-
	+25°C	a, nm	0.2970	0.2967	0.2967	0.2967	0.2967	0.2967	-
		c, nm	0.4700	0.4700	0.4700	0.4700	0.4700	0.4700	-
		crystallite size, nm	8 ±2	8 ±2	8 ±2	10 ±3	10 ±3	12 ±3	-
		wt% Rietveld	13.7	11	7.5	3.2	1.6	0.8	0
hexagonal (Sn, Cu,Ni)Ti$_3$ space group P63/mmc	-78°C	a, nm	0.5894	0.5908	0.5908	0.5908	0.5908	0.5908	0.5908
		c, nm	0.4759	0.4763	0.4763	0.4763	0.4763	0.4763	0.4763
		crystallite size, nm	20 ±6	8 ±2	8 ±2	8 ±2	3 ±1	5 ±1	2 ±1
		wt% Rietveld	14.2	15.1	7.6	7.3	13.4	9.9	7.9
	+25°C	a, nm	0.5894	0.5890	0.5890	0.5923	0.6303	0.6157	0.5834
		c, nm	0.4759	0.4765	0.4765	0.4764	0.4741	0.4730	0.5080
		crystallite size, nm	21 ±3	11 ±3	9 ±2	9 ±2	3 ±1	2 ±1	~1.0
		wt% Rietveld	14.2	20.9	9.8	6.0	10.5	17.3	29.1

Table continues on the next page

Table continued from the previous page

Phase	Temp	Parameter							
tetragonal (Cu, Sn)Ti$_3$ space group P4/mmm	-78 °C	a, nm	0.4150	0.4246	0.4246	0.4246	0.4246	0.4246	0.4246
		c, nm	0.3580	0.3496	0.3496	0.3496	0.3496	0.3496	0.3496
		crystallite size, nm	8 ±2	9 ±3	4 ±1	4 ±1	3 ±1	3 ±1	2 ±1
		wt% Rietveld	5.8	9.6	22.2	14.8	6.2	25.6	17.4
	+25°C	a, nm	0.4150	0.4250	0.4219	0.4250	0.4250	0.4222	0.4250
		c, nm	0.3580	0.3500	0.3552	0.3535	0.3582	0.3600	0.3510
		crystallite size, nm	8 ±2	4 ±1	3 ±1	3 ±1	2 ±1	2 ±1	2 ±1
		wt% Rietveld	5.8	15.0	22.0	17.2	13.7	35.0	25.7
cubic α-Iron space group Im-3m	-78°C	a, nm	-	0.2874	0.2875	0.2874	0.2876	0.2875	0.2874
		crystallite size, nm	-	8 ± 2.0	8 ± 2	8 ±2	9 ±2	10 ±2	9 ±2
		wt% Rietveld	-	4.8	5.1	6.1	10.0	7.1	9.5
	+25°C	a, nm	-	0.2872	0.2873	0.2873	0.2873	0.2876	0.2883
		crystallite size, nm	-	13 ± 3	12 ±3	9 ±2	13 ±3	8 ±2	8 ±2
		wt% Rietveld	-	2	3.8	4.2	2.3	0.7	0.7
amorphous		-78 °C	3	6	30	31	33	27	32
		+25 °C	3	5	25	34	36	28	24
R_{exp}		-78 °C	22.53	17.77	17.00	15.96	14.80	15.76	14.22
		+25 °C	22.53	18.20	20.48	19.90	17.47	14.44	16.06
R_{wp}		-78 °C	28.14	19.86	17.40	16.31	15.21	16.16	14.69
		+25 °C	28.14	19.40	21.38	20.63	17.98	15.10	16.33
Sigma		-78 °C	1.25	1.12	1.02	1.02	1.03	1.03	1.03
		+25 °C	1.25	1.07	1.04	1.04	1.03	1.05	1.02

variations could not be detected by the XRD.

One significant index of fitting results was the R-Bragg index, a goodness of fit index for single-phase calculations, which was a dimensionless number; the best fit was given by the value of 1. The results had good R-Bragg values, well within common values for Rietveld refinement, except for 180 min of milling. This step coincided with the recrystallization/amorphization period, suggesting that nanocrystalline phases might be higher in number but similar in structure to those observed by the XRD, e.g., phases developed in high dislocation density zones and grain boundaries. However, identification and quantification of these phases were beyond the field of regular phase analysis and required more detailed investigations, being out of the scope of this paper.

Period I:

The changes in the phase amounts offered new insights (Table 1) into the phenomenon, as a function of the milling time. Cross-section BSE micrographs of powders shown in Fig. 1 represented an evidence of a complex phase distribution. The bright phase corresponded to the Sn contain phases, while the dark phase corresponded to the other crystalline and amorphous phases (Fig.2). A very significant change occurred for the cubic Cu(Ni, Cu)Ti$_2$ phase based on the XRD analysis at both milling temperatures. After 30 minutes, 74 % of the initial quantity of the cubic Cu(Ni, Cu)Ti$_2$ phase partly transformed to the orthorhombic structure, the other part of the atoms was incorporated into the amorphous structure, (Sn,Cu,Ni)Ti$_3$ and (Cu,Sn)Ti$_3$ phase at room temperature milling (Table 1). The situation was different at -78 °C milling: 82 % of the initial quantity of this phase almost completely transformed into an orthorhombic structure (Table 1). In the Cu-Ni-Ti system, there was a wide composition range where the

alloys had the thermoelastic martensitic transformation [25, 26]. The martensitic transformation temperature of ternary $Ti_{49}Ni_{26}Cu_{25}$ (at.%) composition was 40 °C [27]. The body-centered structure transformed without diffusion into an orthorhombic structure during the cooling process. The orthorhombic phase was stable within a certain composition range in the ternary system at low temperature [25]. In our case, the chemical composition calculated from the Rietveld refinement was $Cu(Ni_{0.7}Cu_{0.3})Ti_2$ ($Ti_{50}Ni_{17.5}Cu_{32.5}$ at.%). During the high-energy ball milling, the powder particles were trapped between colliding media, and the kinetic energy of the media was dissipated as stressing energy. When the stressing energy reached a critical value, then the structure transformation occurred to reduce the Gibbs free energy. The investigation could indicate the nano-scaled stress-induced transformation in this phase based on the XRD measurement. A deformation-induced martensite phase was reported to be formed in mechanically alloyed Cu-Zn alloy powders [28, 29], and stainless steels [30, 31]. At -78 °C, the cubic structure transformation to orthorhombic was greater in degree. Considering the length of *a*, *b*, and *c*, the unit cell dimensions of this orthorhombic phase decreased after 30 min of milling, and the crystallite size decreased to one-third. The same transformation of BCC to orthorhombic structures was published for the Ti-Al-Nb system [32].

The amount of the hexagonal a-Ti(Cu) phase disappeared after 30 min of milling (Table 1). The amount of the hexagonal (Sn, Cu, Ni)Ti$_3$ phase increased at room temperature milling process. The amount of the other Sn-containing phase, (Cu, Sn)Ti$_3$ increased (Table 1), but the crystallite size increased at lower temperature and decreased at room the temperature (Fig.4). Unit cell size changed, *a* parameter increased from 0.4150 to 0.4246 nm, while *c* decreased from 0.350 to 0.3496 nm at the lower temperature. This inferred that the composition of this phase changed. The crystallite sizes of all phases decreased after 30 min of milling except the (Cu, Sn)Ti$_3$ phase at lower temperature milling (Fig.4).

The a-Fe content should be considered as contamination material caused by the milling process and coming from the milling media.

The amorphous phase was 5 wt.% at the end of Period I at both milling temperatures (Table 1).

The average hardness of the particles (which were embedded in acrylic resin), increased (from 506 HV to 550 -590 HV$_{0.01}$) as can be seen in Fig. 5. The particles were fractured owing to the large shear deformations in some cases.

Period II:

The amount of the cubic and orthorhombic $Cu(Ni,Cu)Ti_2$ phase decreased after 60 min of milling at both temperatures.

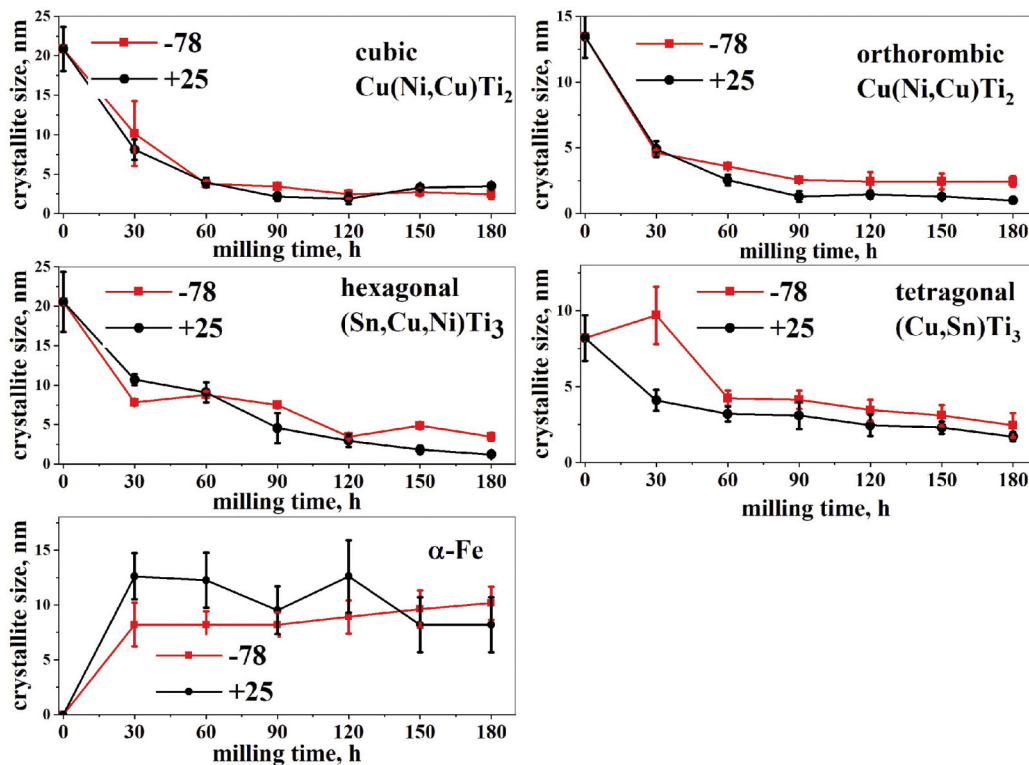The crystallite size decreased almost exponentially (Fig.4) at both milling temperatures.

Figure 4. *Effect of milling time on the crystallite size*

The amount of the orthorhombic Cu(Ni, Cu)Ti$_2$ phase first decreased to 24.8 and 31.4 wt% after 60 min milling and after that it increased up to 34.3 wt% after 120 min at both temperature milling. The crystallite size of the orthorhombic Cu(Ni,Cu)Ti$_2$ phase decreased continuously up to 120 min of milling.

The weight fraction of the hexagonal (Sn,Cu,Ni)Ti$_3$ phase decreased by 90 min of milling and slightly increased up to 120 min at both milling temperatures (Table 1). The crystallite size decreased at both milling temperatures (Fig.4).

It has to be noted, that the amount of the (Cu,Sn)Ti$_3$ phase increased up to 60 min of milling and between 60 and 120 min it decreased (Table 1). The crystallite size was reduced continuously (Fig.4).

Thermodynamic formula of transformation from crystalline to amorphous state can be given as follows:

$$\Delta G = \Delta H - T \cdot \Delta S \qquad (1)$$

Here, ΔG refers to Gibbs free energy; ΔH shows the formation enthalpies; and ΔS means formation entropies in an alloy system. The amorphous phase formed when ΔH was low and ΔS was high simultaneously. During the high-energy milling process, ΔS increased gradually. It required storing sufficient energy in the crystalline compounds to overcome the energy barrier (normally around 5 kJ/mole [33]) for amorphisation. The structural defects (such as vacancies, dislocations, grain boundaries and anti-phase boundaries, and disordering of the crystal structure) increased the energy of the milled powders.

The sum of cubic, orthorhombic Cu(Ni,Cu)Ti$_2$ structures and α-Ti decreased steeply up to 60 minutes and then decreased to a lesser extent for 150 minutes at both temperatures, while the weight fraction of the amorphous phase(s) was from 5 to 31

and 36 at -78 °C and +25 °C milling, respectively (Table 1). This can be explained if these three crystalline structures at least partly transformed into an "X-ray amorphous structure" (hereinafter referred to as an amorphous structure). According to the loss of crystalline phases, Ti, Cu, and Ni atoms mostly created an amorphous structure. Modeling the amorphous components or "short-range ordered phases" with the peak fitted to the halo (hump) method was useful and allowed the extraction of information about the composition of amorphous phases and size range of domains with different compositions. Observing the amorphous halo, the maximum position of the halo reflected the most frequent distances between atoms, so the peak corresponding to smaller angles corresponded to the amorphous phase with the largest distances between atoms [35]. In this system, the larger atoms were Sn and Ti, while Cu or Ni were smaller atoms (Table 2). The first peak position of the amorphous halo decreased between 60 and 120 min of milling at room temperature milling, which meant that the chemical composition of short-range ordered phases changed (Fig.6). In contrast, the change was exactly the opposite at -78 °C, the peak position slightly increased. After 60 min of milling, the appearance of the second peak in the amorphous halo indicated the formation of a second short-range ordered phase in the amorphous content, at both milling temperatures (Table 3). In this system, the atomic scattering factors of Ti and Cu were nearly equal; namely, the appearance of inhomogeneity areas was much more pronounced [34]. This second short-range ordered phase was probably enriched in Cu and/or Ni and its development coincided with the quantity reduction of the weight fraction of all crystalline phases except the (Sn,Cu,Ni)Ti$_3$ and Fe phases (Table 1). The amorphous content reached the maximum value after 120 min at both temperature milling.
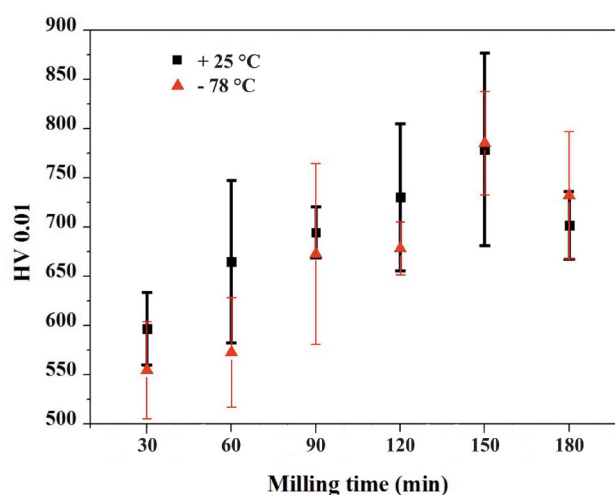

***Figure 5.** Effect of milling time on hardness*

Namely, more Cu, Ni, and Ti atoms and Sn atoms could transfer into other phases at -78 °C milling. The crystallite size was 2.7-4.2 nm after 180 min of milling (Fig.4).

The a-Fe content increased with the milling time (Table 1) for both temperatures, with higher values at low-temperature milling up to 90 min. This process occurred due to the increased ductility of milled material at low temperatures. After 90 min of milling the a-Fe content began to decrease, suggesting its incorporation into the milled material by mechanical alloying at room temperature milling. The average hardness of particles increased continuously (up to 670-775 $HV_{0.01}$) (Fig.5). The standard deviation of hardness was generally large due to the many different phases in the composites.

Period III:

The sum amount of the cubic, orthorhombic $Cu(Ni,Cu)Ti_2$ phase decreased after 120 min at both temperature milling. (Table 1). Due to this decrease, there were Cu, Ni, and Ti atoms that could be transferred with diffusion into other phases. The crystallite size of both $Cu(Ni,Cu)Ti_2$ phases was below 5 nm (Fig.4).

Temperature played a major role in changing the amount of $(Sn,Cu,Ni)Ti_3$ phase between 120 and 180 min. The weight percent of the $(Sn,Cu,Ni)Ti_3$ phase varied differently at the two temperatures of milling (Table 1). At room temperature milling the amount of this phase was double, while the crystallite size was 1.2 nm after 180 min of milling (Fig.4). The weight fraction of this phase decreased at lower temperature milling. Namely, more Cu, Ni, and Ti caused the quantity of a-Fe content to decrease suddenly after 120 min at both temperature milling indicating that Fe atoms were dissolved in both the crystalline and amorphous phases. When the Fe content decreased, the amorphous fraction also decreased at both temperature milling, which meant that Fe contamination could induce the crystallization processes of the amorphous phase [35]. However, at

lower temperature milling, the amount of a-Fe increased after 150 min and the amount of amorphous phase also increased, because low temperature inhibited crystallization.

In the period from 120 and 180 min of milling a big change was observed in the amount of the $(Cu,Sn)Ti_3$ phase (Table1). The weight fraction of this phase first increased after 150 min at both milling temperatures and due to further milling, its weight fraction depended on the milling temperature: at room temperature milling weight fraction continuously increased, while at -78 °C milling decreased. This phenomenon could be explained by the slow diffusion possibility of Sn atoms at lower temperatures, due to their large atomic radius.

In the third period, mechanical crystallization occurred at room temperature milling and the amorphous phase in-situ crystallized. Contamination such as Fe, Cr, and oxygen could promote crystallization owing to chemistry change. The Fe content decreased to 0.7 wt% after 180 min probably due to mechanical alloying of milling media and, in parallel, the amorphous content was greatly reduced (24 wt%) at room temperature milling. In the case of milling at low temperature, the Fe content increased up to 9.5 wt% and the amorphous quantity was unchanged (32 wt%). As can be seen in Fig.5, the hardness of the particles increased continuously up to 150 min of milling (with a 780 $HV_{0.01}$ peak value). The 1.5x increase in hardness was produced by the development of high dislocation density [17] and phase transformations after 150 min of milling. The change in hardness values had a similar trend with amorphous evolution and recrystallization. Fig.8 illustrates the DSC scans for the amorphous-nanocrystalline $Ti_{50}Cu_{25}Ni_{20}Sn_5$ alloy samples after 180 min of milling. It should be mentioned that the crystallization peak observed for amorphous materials obtained by high-energy MM was usually wider and less intense than the corresponding one for cast bulk metallic glasses or MA [36].
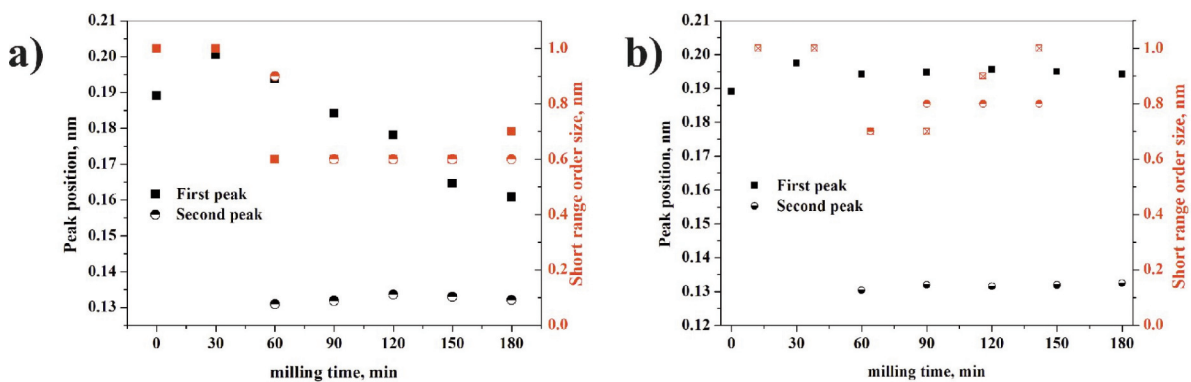

Figure 6. *Features of the amorphous phase in the course of different milling processes based on XRD measurement: a) 25 °C, b)-78 °C*

The DSC trace of the partly amorphous alloy after 180 min of milling was slightly different from the DSC trace of the melt-spin [21] or mechanical alloying [37] sample with the same nominal composition. Two overlapping exothermic peaks could be observed indicating multistage crystallization events in the case of room temperature milling. However, the crystallization process of the amorphous phase took place differently in the case of milling at -78 °C, indicating that the amorphous structure was different. This conclusion confirmed the XRD data regarding amorphous structure (Table 3), which suggested more Sn and Ti in the amorphous phase for the -78 °C samples by the higher maximum value of the amorphous halo. The two crystallization processes for the room temperature sample in Fig.8 were related to the difference of Cu-Ni and Sn-Ti
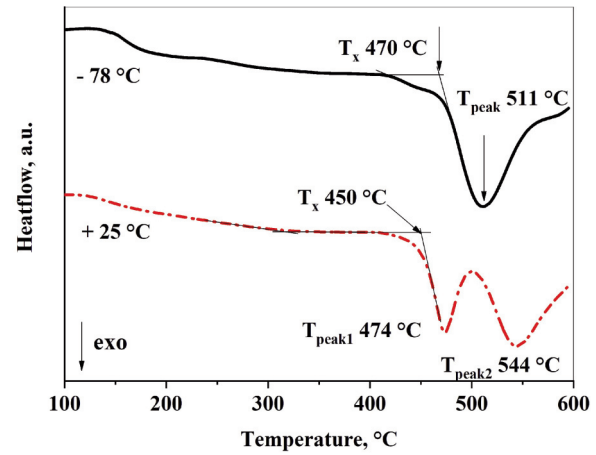

Figure 8. *DSC curves of $Ti_{50}Cu_{25}Ni_{20}Sn_5$ alloy after180 min of milling time (heating rate 40°C/min)*
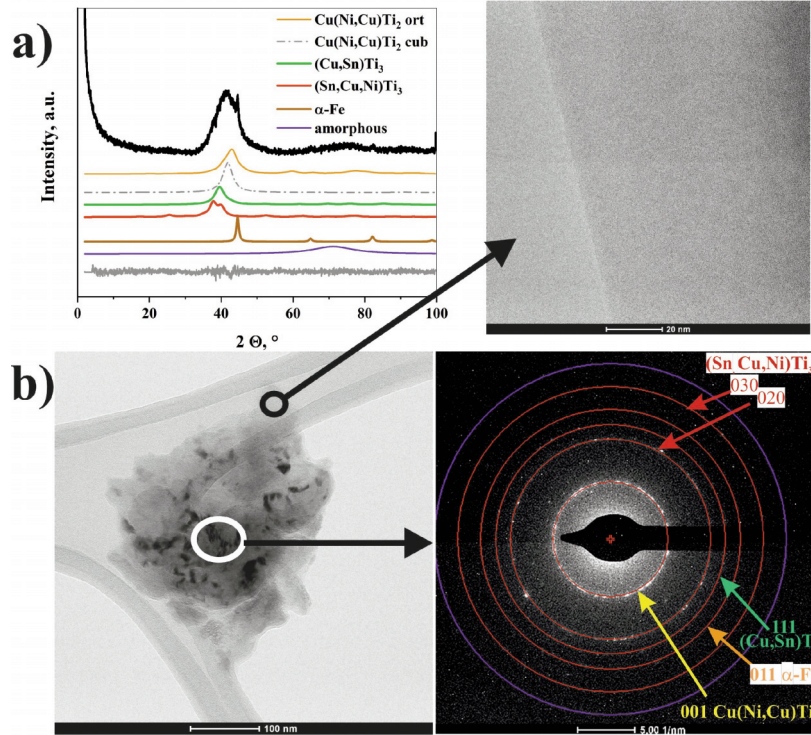

Figure 7. *XRD pattern (a) and bright field TEM images of 180 min milled at -78 °C particle (b) TEM image, HRTEM image, and selected area diffraction pattern (SAED). The place of the HRTEM image (the black circle) and diffraction pattern (the white circle) is marked on the image*

Table 2. *Calculated impurity and self-diffusion coefficient based on the pre-exponential factor (D_0) and activation energy (E) for diffusion in a-titanium*

Diffusing atom	atomic radius, nm	D_0, m²/s	E, kJ/mol	Method	$D_{+25\,°C}$ / $D_{-78\,°C}$	Reference
Sn	0.1620	$4.0×10^{-3}$	338	substitutional	$1.9×10^{31}$	[41]
		$7.27×10^{-6}$	256	solute-vacancy complex	$5.0×10^{23}$	[38]
Ti	0.1462	$1.7×10^{-8}$	193	-	$7.4×10^{17}$	[40]
Cu	0.1278	$3.8×10^{-5}$	195	-	$1.1×10^{18}$	[40]
Ni	0.1246	$5.4×10^{-6}$	142	-	$1.4×10^{13}$	[40]

ratios in the amorphous phase, as evidenced by the amorphous halo characteristics (Table 3). At 450 °C and 470 °C, not only the phase separation of the amorphous content started but the grain growth of nanocrystals started as well. Both processes were exothermic reactions.

The concentration and the diffusion coefficient together influenced the diffusion flux according to Fick's law. The diffusion coefficient in Fick's first and second law determined the rate of diffusion:

$$D = D_0 exp\left[-\frac{E}{RT}\right] \quad (2)$$

where D diffusion coefficient [m²/s], D_0 pre-exponential [m²/s], E activation energy [J/mol or eV/atom], R gas constant [8.314 J/mol-K], and T absolute temperature [K]. Different elements showed different diffusion behaviors in the same alloy. Pre-exponential depended on diffusion direction [38], on mechanisms (e.g., the interstitial diffusion mechanism and solute-vacancy complex mechanism) [39], and the size of atoms [40].

In the investigated alloy the most present atom was Ti, so as an estimate, the diffusion of the constituents in alpha titanium was examined. Diffusion data for the a-Ti -Sn system is extremely limited in the literature. To the best knowledge of the authors, no experimental interdiffusion coefficients at -78 °C are available in the literature currently. Some data on D_0 and E for the diffusion in a-Ti are listed in Table 3. However, it should be noted that the diffusion along the grain boundaries can be many orders of magnitude higher than in the bulk. In nanocrystalline materials, where the grain size is about 10 nm, the number of atoms being in grain boundaries can be higher than about 20 at.%. Moreover, the diffusion at the interface between the amorphous and crystalline phases is even greater especially if energy is transmitted to the matter by milling. In an amorphous structure, interstitial-like diffusion is also possible, so the atomic radius is an important factor, a small radius accelerates diffusion. The fast diffusers are characterized by their large pre-exponential factors. However, activation energy is also a determining factor. As can be seen from the data on Sn, the pre-exponential of the substitutional mechanism was higher than the solute-vacancy complex mechanism. Nevertheless, Sn diffused mainly through normal vacancy mediated mechanism due to the high substitutional to interstitial preferential energy [39]. The fast diffuser atoms were Cu and Ni and the slow diffusor was Sn which had the largest atomic radius based on Table 2.

Temperature was also a determining factor of the diffusion coefficient. Observing the ratio of the
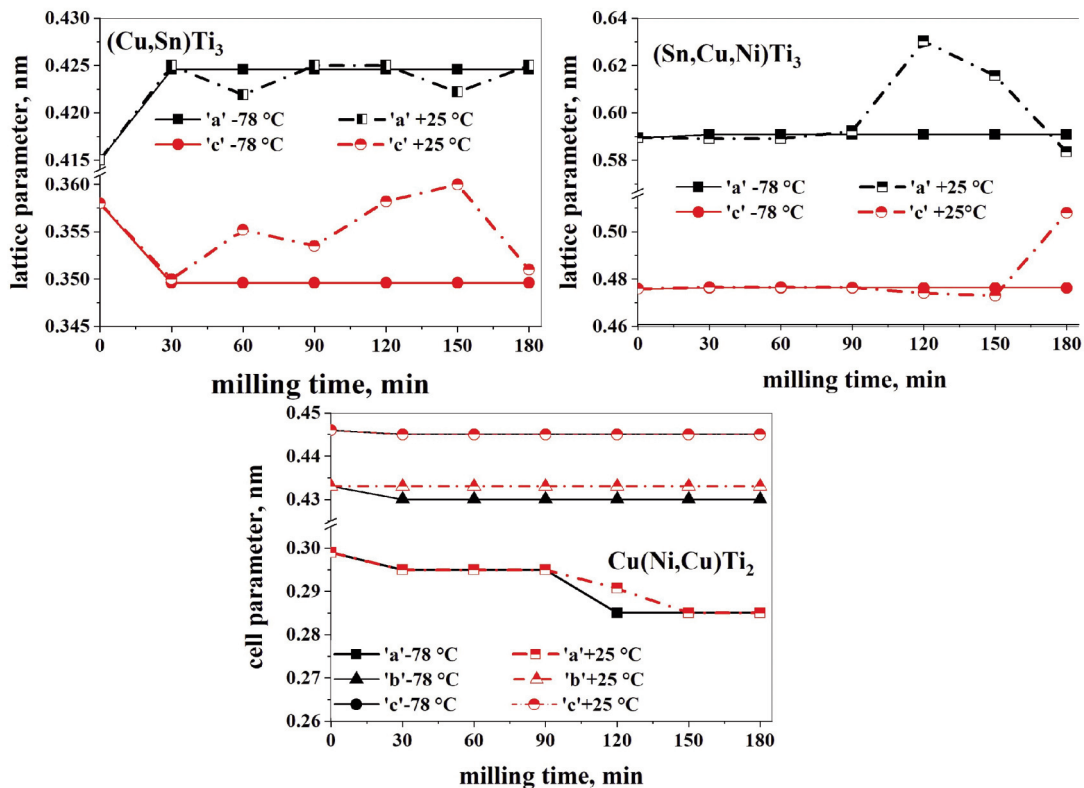

Figure 9. *Changes in cell parameters 'a' (square), 'b' triangles and 'c' (circles) of tree phases during milling at -78 °C (full line) and +25 °C (dotted line)*

Table 3. *Features of amorphous structure based on the XRD in the case of Ti₅₀Cu₂₅Ni₂₀Sn₅ alloy*

milling time, min		amorphous fraction, wt%	amorphous halo			
			first peak		second peak	
			position, nm	domain size, nm	position, nm	domain size, nm
0		3	0.1890	1.0	-	-
30	-78°C	5	0.1974	0.7	-	-
	+25°C	5	0.2006	1.0	-	-
60	-78°C	25	0.1942	0.7	0.1304	0.7
	+25°C	25	0.1938	0.8	0.1309	0.9
90	-78°C	31	0.1947	0.7	0.1320	0.8
	+25°C	34	0.1841	0.6	0.1318	0.6
120	-78°C	33	0.1956	0.9	0.1316	0.8
	+25°C	36	0.1781	0.6	0.1336	0.6
150	-78°C	27	0.1950	1.0	0.1319	0.8
	+25°C	28	0.1646	0.6	0.1330	0.6
180	-78°C	32	0.1931	0.7	0.1331	0.7
	+25°C	24	0.1608	0.7	0.1321	0.6

diffusion coefficients calculated at 25 °C and -78 °C, it can be stated that the temperature had the greatest effect on the diffusion of Sn. Changes in unit cell parameters (Fig.9) of two Sn-containing phases and $Cu(Ni,Cu)Ti_2$ phase highlighted the difference in diffusivity of Sn compared to Ni and Cu. It can be established, that the changes were much greater when grinding at room temperature in the case of Sn-containing phases. However, the cell parameter change of $Cu(Ni,Cu)Ti_2$ phase depended less on milling temperature, probably because Cu and Ni were fast diffuser atoms, less affected by temperature compared to Sn.

4. Conclusions

Amorphous-nanocrystalline composite was produced by high energy ball-milling of $Ti_{50}Cu_{25}Ni_{20}Sn_5$ alloy at room temperature and -78 °C. During the high energy ball-milling, mechanical alloying process was initiated and progressed to recrystallization. The following main conclusions can be drawn:

1. An amorphous structure with nanocrystalline phases was produced after a short milling time due to intense shearing and plastic deformation induced by the mechanical effect of balls at both temperatures. The amorphous content was only slightly higher at room temperature milling (33 wt% at -78 °C and 36 wt% at +25 °C). However, the mechanical crystallization was lower for the -78 °C milling process.

2. Two short-range ordered phases could be distinguished based on the X-ray diffraction, indicating atomic segregation in the transforming solid phases in the case of both milling temperatures. The composition of "short-range ordered phases" changed during the milling process and depended on the milling temperature based on the XRD investigation and thermal process investigation.

3. The crystallite size decreasing depended not only on the composition, but on the milling temperature too. The interval of crystallite size was between 1.2 and 11.7 nm after 180 min of milling.

4. The TEM investigation confirmed that an agglomerate consisted of some particles with different compositions. The sub-particle sizes were between 10-50 nm after 180 min of milling time.

5. Stress-induced phase transformation occurred during the first 30 minutes of milling. Cubic $Cu(Ni,Cu)Ti_2$ structure was transformed into an orthorhombic structure owing to the shear/stress, dislocations, and Cu substitution during both milling processes.

Authors contribution

F. Kristaly: Conceptualization, Investigation, Methodology, Writing – original draft, Writing – review & editing. M. Sveda: Resources, Investigation. A. Sycheva: Investigation. T. Miko, A. Racz, G. Karacs: Methodology. D. Janovszky: Supervision, Conceptualization, Writing – review & editing.

Conflicts of interest

The authors declare that they have no known competing financial interests or personal relationships that could have appeared to influence the work reported in this paper.

References

[1] J. Fan, F. Wu, D. Li, Dynamic compressive response of a dendrite-reinforced Ti-based bulk metallic glass composite, Materials Science and Engineering: A, 720 (2018) 140-144. https://doi.org/10.1016/j.msea.2018.02.071

[2] P. Gong, L. Deng, J. Jin, S. Wang, X. Wang, K. Yao, Review on the research and development of Ti-based bulk metallic glasses, Metals, 6 (2016) 264. https://doi.org/10.3390/met6110264

[3] S. Bera, B. Sarac, S. Balakin, P. Ramasamy, M. Stoica, M. Calin, J. Eckert, Micro-patterning by thermoplastic forming of Ni-free Ti-based bulk metallic glasses, Materials & Design, 120 (2017) 204-211. https://doi.org/10.1016/j.matdes.2017.01.080

[4] L. E. Tanner, R. Ray, Physical properties of Ti50Be40Zr10 glass, Scripta Metallurgica, 11 (1977) 783-789. https://doi.org/10.1016/0036-9748(77)90076-X

[5] P. Gong, S. Wang, Z. Liu, W. Chen, N. Li, X. Wang, K.F. Yao, Lightweight Ti-based bulk metallic glasses with superior thermoplastic formability, Intermetallics, 98 (2018) 54–59. https://doi.org/10.1016/j.intermet.2018.04.019

[6] A. Inoue, Bulk amorphous and nanocrystalline alloys with high functional properties, Materials Science and Engineering: A, 304-306 (2001) 1-10. https://doi.org/10.1016/S0921-5093(00)01551-3

[7] D. Roy, R. Mitra, T. Chudoba, Z. Witczak, W. Lojkowski, H.-J. Fecht, I. Manna, Structure and mechanical properties of Al65Cu20Ti15-based amorphous/nanocrystalline alloys prepared by high-pressure sintering, Materials Science and Engineering: A, 497 (2008) 93-100. https://doi.org/10.1016/j.msea.2008.07.059

[8] M.M. Li, A. Inoue, Y. Han, F.L. Kong, S.L. Zhu, E. Shalaan, F. Al-Marzouki, Influence of Ag replacement on supercooled liquid region and icosahedral phase precipitation of Zr65Al7.5Ni10Cu17.5-xAgx (x = 0–17.5 at%) glassy alloys, Journal of Alloys and Compounds, 735 (2018) 1712-1721. https://doi.org/10.1016/j.jallcom.2017.11.203

[9] E. Chicardi, C. García-Garrido, M.J. Sayagués, Y. Torres, V. Amigó, C. Aguilar, Development of a novel fcc structure for an amorphous-nanocrystalline Ti-33Nb-4Mn (at.%) ternary alloy, Materials Characterization, 135 (2018) 46-56. https://doi.org/10.1016/j.matchar.2017.11.021

[10] K. A. Nazari, A. Nouri, T. Hilditch, Compressibility of a Ti-based alloy with varying amounts of surfactant prepared by high-energy ball milling, Powder Technology 279 (2015) 33-41. https://doi.org/10.1016/j.powtec.2015.03.044

[11] I. Manna, P. P. Chattopadhyay, F. Banhart, H. J. Fecht, Development of amorphous and nanocrystalline Al65Cu35−xZrx alloys by mechanical alloying, Materials Science and Engineering: A, 379 (2004) 360-365. https://doi.org/10.1016/j.msea.2004.03.010

[12] G. L. Caër, P. Delcroix, S. B. Colin, T. Ziller, High-energy ball-milling of alloys and compounds, Hyperfine Interactions, 141 (2002) 63-72. https://doi.org/10.1023/A:1021245701811

[13] C. C. Koch, J. D. Whittenberger, Mechanical milling/alloying of intermetallics, Intermetallics 4 (1996) 339-335. https://doi.org/10.1016/0966-9795(96)00001-5

[14] C. Suryanarayana, Mechanical alloying and milling, Progress in Materials Science, 46 (2001) 1-184. https://doi.org/10.1016/S0079-6425(99)00010-9

[15] H. Kishimura, H. Matsumoto, Fabrication of Ti–Cu–Ni–Al amorphous alloys by mechanical alloying and mechanical milling, Journal of Alloys and Compounds, 509 (2011) 4386-4389. https://doi.org/10.1016/j.jallcom.2010.12.181

[16] W. T. Qiu, Y. Pang, Z. Xiao, Z. Li, Preparation of W-Cu alloy with high density and ultrafine grains by mechanical alloying and high pressure sintering, International Journal of Refractory Metals and Hard Materials, 61 (2016) 91–97. https://doi.org/10.1016/j.ijrmhm.2016.07.013

[17] C. Aguilar, F. Castro, V. Martínez, D. Guzmán, F. de las Cuevas, L. Lozada, N. Vielma, Structural study of nanocrystalline solid solution of Cu–Mo obtained by mechanical alloying, Materials Science and Engineering: A, 54 (2012) 189–194. https://doi.org/10.1016/j.msea.2012.03.105

[18] S. Sugimoto, T. Niwa, Y. Nakanishi, K. Danjo, Development of a novel ultra cryo-milling technique for a poorly water-soluble drug using dry ice beads and liquid nitrogen, International Journal of Pharmaceutics, 426 (2012) 162–169. https://doi.org/10.1016/j.ijpharm.2012.01.007

[19] T. Zhang, A. Inoue, Thermal and mechanical properties of Ti–Ni–Cu–Sn amorphous alloys with a wide supercooled liquid region before crystallization, Materials Transactions, JIM, 39 (1998) 1001-1006. https://doi.org/10.2320/matertrans1989.39.1001

[20] Y. Cho, C. Koch, Mechanical milling of ordered intermetallic compounds: the role of defects in amorphization, Journal of Alloys and Compounds, 194 (1993) 287-294. https://doi.org/10.1016/0925-8388(93)90013-D

[21] M. Imani, M. Enayat, Investigation of amorphous phase formation in Fe-Co-Si-B-P - thermodynamic analysis and comparison between mechanical alloying and rapid solidification experiments, Journal of Alloys and Compounds, 705 (2017) 462-467. https://doi.org/10.1016/j.jallcom.2017.02.100

[22] P. Gong, S. Wang, Z. Liu, W. Chen, N. Li, X. Wang,

K.F. Yao, Lightweight Ti-based bulk metallic glasses with superior thermoplastic formability, Intermetallics, 98 (2018) 54–59.
https://doi.org/10.1016/j.intermet.2018.04.019

[23] Y. Kim, W. Kim, D. Kim, A development of Ti-based bulk metallic glass, Materials Science and Engineering: A, 375-377 (2004) 127-135.
https://doi.org/10.1016/j.msea.2003.10.115

[24] D. Janovszky, F. Kristaly, T. Miko, A. Racz, M. Sveda, A. Sycheva, T. Koziel, Phase transformation and morphology evolution of Ti50Cu25Ni20Sn5 during mechanical milling, Materials, 11 (2018) 1769.
https://doi.org/10.3390/ma11091769

[25] W. Tang, R. Sandström, Z. G. Wei, S. Miyazaki, Experimental investigation and thermodynamic calculation of the Ti-Ni-Cu shape memory alloys, Metallurgical Materials Transactions A, 31 (2000) 2423-2430. https://doi.org/10.1007/s11661-000-0187-y

[26] J. Frenzel, A. Wieczorek, I. Opahle, B. Maaß, R. Drautz, G. Eggeler, On the effect of alloy composition on martensite start temperatures and latent heats in Ni–Ti-based shape memory alloys, Acta Materialia, 90 (2015) 213–231.
https://doi.org/10.1016/j.actamat.2015.02.029

[27] G. Pan, C. Balagna, L. Martino, J. Pan, S. Spriano, Microstructure and transformation temperatures in rapid solidified Ni–Ti alloys. Part II: The effect of copper addition, Journal of Alloys and Compounds, 589 (2014) 633–642.
https://doi.org/10.1016/j.jallcom.2013.09.212

[28] S. Pabi, B. Murty, Mechanism of mechanical alloying in Ni-A and Cu-Zn systems, Materials Science and Engineering: A, A214 (1996) 146-52.
https://doi.org/10.1016/0921-5093(96)10224-0

[29] B. McDermott, C. Koch, Preparation of beta brass by mechanical alloying of elemental copper and zinc, Scripta Metallurgica, 20 (1986) 669-72.
https://doi.org/10.1016/0036-9748(86)90487-4

[30] H. Kotan, Microstructural evolution of 316L stainless steels with yttrium addition after mechanical milling and heat treatment, Materials Science and Engineering: A, 647 (2015) 136-143.
https://10.1016/j.msea.2015.09.011

[31] C. Kuhrt, L. Schultz, Phase formation and martensitic transformation in mechanically alloyed nanocrystalline Fe-Ni, Journal of Applied Physics, 73 (4) (1993) 1975-1980. https://doi.org/10.1063/1.353162

[32] L. A. Bendersky, A. Roytburd, W. J. Boettinger, Transformation of BCC and B2 high temperature phases to HCP and orthorhombic structures in the Ti-Al-Nb system, part I: microstructural predictions based on a subgroup relation between phases, Journal of Research of the National Institute of Standards and Technology, 98 (1993) 561-583.
https://doi.org/10.6028/jres.098.038

[33] D.L. Zhang, Processing of advanced materials using high-energy mechanical milling, Progress in Materials Science, 49 (2004) 537–560.
https://doi.org/10.1016/S0079-6425(03)00034-3

[34] G. Abrosimova, A. Aronin, Amorphous and nanocrystalline metallic alloys, Progress in Metallic Alloys, (V. Glebovsky Editor), IntechOpen, 2016.
https://doi.org/10.5772/64499

[35] T. Yamamoto, T. Takahashi, H. Kimura, A. Inoue, Effect of ball-milling and shot-peening on Zr55Al10Ni5Cu30 alloys, Journal of Alloys and Compounds, 430 (2007) 97-101.
https://doi.org/10.1016/j.jallcom.2006.04.050

[36] S. Scudino, M. Sakaliyska, K.B. Surreddi, J. Eckert, Mechanical alloying and milling of Al–Mg alloys, Journal of Alloys and Compounds, 483 (2009) 2-7.
https://doi.org/10.1016/j.jallcom.2008.07.161

[37] N. Oanh, P. Choi, J. Kim, D. Kwon, Y. Kwon, Thermal stability of amorphous Ti-Cu-Ni-Sn prepared by mechanical alloying, Materials Science Forum, 534-536 (2007) 233-236.
https://doi.org/10.4028/www.scientific.net/MSF.534-536.233

[38] W. Xu, S. Shang, B. Zhou, Y. Wang, L. Chen, C. Wang, X. Liu, Z. Liu, A first-principles study of the diffusion coefficients of alloying elements in dilute α-Ti alloys, Physical Chemistry Chemical Physics, 18 (2016) 16870-16881. https://doi.org/10.1039/C6CP01899H

[39] L. Zhang, Z. Chen, Q. Hu, R. Yang, On the abnormal fast diffusion of solute atoms in α-Ti: a first-principles investigation, Journal of Alloys and Compounds, 740 (2018) 156-166.
https://doi.org/10.1016/j.jallcom.2017.12.359

[40] O. Taguchi, Y. Iijima, Diffusion of copper, silver and gold in α-titanium, Philosophical Magazine A, 72 (1995) 1649-1655.
https://doi.org/10.1080/01418619508243935

[41] R.A. Pérez, F. Dyment, M. Behar, Diffusion of Sn in different purity α-Ti, Materials Letters, 57 (2003) 2670-2674.
https://doi.org/10.1016/S0167-577X(02)01353-8

UTICAJ TEMPERATURE MLEVENJA I VREMENA NA FORMIRANJE FAZA KOD LEGURE NA BAZI Ti

F. Kristaly [a], M. Sveda [b], A. Sycheva [b], T. Miko [c], A. Racz [d], G. Karacs [b], D. Janovszky [b,*]

[a] Institut za mineralogiju i geologiju, Univerzitet u Miškolcu, Mađarska
[b] MTA-ME grupa za istraživanje materijala ELKH, Miškolc, Mađarska
[c] Institut za fizičku metalurgiju, obradu metala i nanotehnologiju, Univerzitet u Miškolcu, Mađarska
[d] Institut za pripremu i preradu sirovina i životnu sredinu, Univerzitet u Miškolcu, Mađarska

Apstrakt

$Ti_{50}Cu_{25}Ni_{20}Sn_5$ (at.%) prah je podvrgnut mlevenju u visoko-energetskom mlinu na sobnoj tempraturi i na -78 °C. Za ispitivanje funkcije vremena mlevenja, procena faza, morfologije i usitnjavanje veličine zrna korišćene su sledeće metode: SEM, XRD, DSC, TEM i PSA. Detektovana je transformacija kristalne u amorfnu strukturu, a zatim i transformacija u nanokristalnu strukturu tokom daljeg postupka mlevenja. Martenzitna transformacija izazvana naprezanjem dogodila se nakon 30 min na obe temperature, dok se kubna $Cu(Ni,Cu)Ti_2$ faza transformisala u ortogonalnu strukturu. Dobijena vrednost za tvrdoću praha je nakon 150 min mlevenja porasla sa 506 na 780 $HV_{0.01}$. Temperatura mlevenja nije značajno uticala na količinu amorfne frakcije (33-36 wt.%), ali je uticala na sastav amorfnog sadržaja. Veličina kristalita se kretala između 1,2 i 11,7 nm nakon 180 min mlevenja. Količina i parametri ćelija faza koje su sadržale Sn su se razlikovale za dva izvedena eksperimenta mlevenja zato što su se i koeficijenti difuzije atoma Sn u velikoj meri razlikovali.

Ključne reči: Amorfno-nanokristalni kompoziti; Masivno metalno staklo na bazi titanijuma; Mlin sa kuglama; Metalurgija praha; Mikrostruktura